THE JOURNAL OF PHYSICAL CHEMISTRY C

Article

pubs.acs.org/JPCC

Structure and Hindered Vibration of Bi^{2+} in the Red-Orange Phosphor SrB_4O_7:Bi

Mathijs de Jong,[†] Andries Meijerink,[†] Zoila Barandiarán,[‡,§] and Luis Seijo*[,‡,§]

[†]Condensed Matter and Interfaces, Debye Institute for Nanomaterials Science, Utrecht University, Princetonplein 5, 3584 CC Utrecht, The Netherlands

[‡]Departamento de Química, and [§]Instituto Universitario de Ciencia de Materiales Nicolás Cabrera, Universidad Autónoma de Madrid, 28049 Madrid, Spain

ABSTRACT: The emission band profile of bismuth-doped SrB_4O_7 is measured with high resolution, and distinct vibronic features are observed at 4.2 K. The energy intervals show an irregular distribution. It is interpreted in the light of ab initio calculations as due to two off-center totally symmetric normal vibrational modes of Bi^{2+}, with harmonic vibrational frequencies $\omega_{1a'}$ = 73 cm^{-1} and $\omega_{2a'}$ = 89 cm^{-1}, the former being hindered by an energy barrier of about one-third of its vibrational frequency. Wave function-based ab initio calculations on the potential energy surfaces corresponding to the off-center displacements of Bi^{2+} are performed in the three lowest states of the $(BiO_9)^{16-}$ cluster embedded in SrB_4O_7. Bi^{2+} is found to move off-center with respect to the Sr site of C_s point symmetry and to stay in the symmetry plane in the three states. It is also found to have two symmetric and one antisymmetric vibrational modes of frequencies spanning a small window around 100 cm^{-1}. Low energy barriers are found in the symmetric mode of lowest vibrational frequency in the ground state and in the first excited state. On the basis of the ab initio potential energy surface scenario, model calculations on the vibrational levels of two perturbed harmonic oscillators give the values of the empirical energy barrier and the vibrational frequencies.

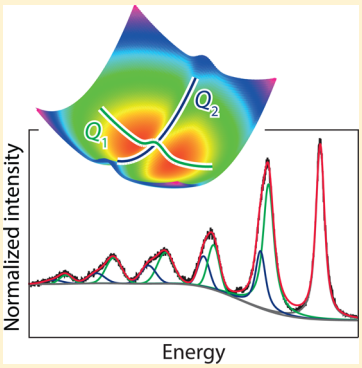

I. INTRODUCTION

Stable divalent bismuth was reported in 1994 to be responsible for the red-orange luminescence of bismuth activated SrB_4O_7 by Blasse et al.[1] This luminescence was attributed to a 6p → 6p emission in Bi^{2+} between two spin−orbit coupling states of the $6s^26p-{}^2P$ term in a low symmetry site: ${}^2P_{3/2}(1) \rightarrow {}^2P_{1/2}$. After that, some work on luminescent materials based on the rarely reported Bi^{2+} ion followed,[2] and now there is a rising interest in these materials driven by the search of new phosphors for energy efficient solid-state lighting devices.[3−7] The knowledge of the electronic structure of Bi^{2+} in solids is very limited, and, as a matter of fact, the only available evidence so far of the existence of stable Bi^{2+} active centers is the spectroscopic measurements. We have started a systematic study on the electronic and geometrical structures of Bi^{2+} in wide band gap solids.

In a separate paper,[8] we add new evidence that support the early assignment of the red-orange luminescence of bismuth-doped strontium tetraborate (SrB_4O_7) to the Bi^{2+} ion in a crystalline phase.[1] Here, we report a combined experimental and ab initio study on the geometrical and vibrational structure of the Bi_{Sr} substitutional defect in SrB_4O_7:Bi^{2+}. The ${}^2P_{3/2}(1) \rightarrow {}^2P_{1/2}$ high-resolution emission spectrum has been measured at 4.2 K, and its fine structure has been found to show an irregular distribution of energy intervals between vibrational levels. The anomalous vibrational structure has been interpreted after ab initio calculations. According to the interpretation, this experiment provides a detailed knowledge of the off-center vibrations of Bi^{2+} in this material.

Besides providing the structural scenario that allows for a detailed understanding of the high-resolution emission spectrum, the ab initio calculations give the off-center displacements of Bi and the characteristics of the corresponding potential energy surfaces (PES) in the ground state and in the two first excited states, which are responsible for the blue absorption that excites the red-orange emission of the material.

This Article is organized as follows: We describe the experiments in section II and the ab initio calculations in section III. The interpretation of the emission spectrum fine structure is discussed in section IV, and the conclusions are presented in section V.

II. EXPERIMENTS

A. Experimental Method. Bismuth doped SrB_4O_7 was prepared as described by Blasse et al.[9] Stoichiometric amounts of $SrCO_3$, H_3BO_3, and Bi_2O_3 for a 0.02% bismuth concentration were mixed and fired in N_2 atm first at 450 °C for 2 h and a second time at 840 °C for 8 h. Only a fraction of the bismuth is in a divalent state, in the order of several ppm.[8]

The high-resolution emission spectrum was measured at 4.2 K by excitation at 480 nm with an Opotek Opolette HE 355II

Received: April 8, 2014
Revised: July 9, 2014
Published: July 9, 2014

   dx.doi.org/10.1021/jp503453y | J. Phys. Chem. C 2014, 118, 17932−17939

tunable laser. For detection we used a Triax 550 monochromator (0.55 m focal length) equipped with a 1200 line grating blazed at 400 nm and a Hamamatsu R928 PMT.

B. Results. The high-resolution emission spectrum is shown in Figure 1. A list of the peak positions is given in the first colum of Table 1. It is clear from this spectrum that the energy intervals between the peaks in the vibronic coupling pattern are irregular and alternating, which is contrary to what is expected from a harmonic oscillator (equidistant peaks) or a slightly anharmonic oscillator (continuous decrease in intervals). In addition to the irregular intervals, all peaks but the zero phonon line are asymmetric.

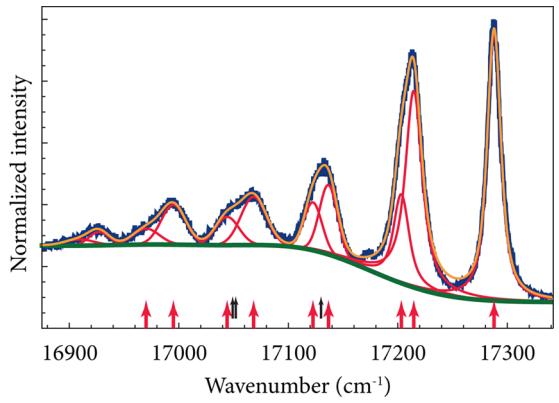

Figure 1. Emission spectrum (blue line) of the $^2P_{3/2}(1) \rightarrow {}^2P_{1/2}$ transition in SrB_4O_7 doped with 0.02% Bi^{2+}, measured at 4.2 K. Excitation is at 480 nm in the $^2P_{3/2}(2)$ level. The total fit (orange line) is obtained by combining a background (green line) with two line profiles for all peaks (red lines), except for the zero phonon line, which was fitted to one line profile. Red arrows indicate the maxima of the fitted line profiles. Black arrows show the expected positions of the (1,1), (1,2), and (2,1) lines in the spectrum.

Table 1. Peak Positions (cm^{-1}) of the Vibronic Coupling in the Emission Spectrum in Figure 1[a]

n	E	ΔE	$E(Q_1)$	$\Delta E(Q_1)$	$E(Q_2)$	$\Delta E(Q_2)$
0	17 287.9					
1	17 213.3	74.6	17 214.6	73.3	17 203.2	84.7
2	17 132.7	80.6	17 136.7	77.9	17 122.5	80.7
3	17 066.6	66.1	17 068.3	68.4	17 044.1	78.4
4	16 993.8	72.8	16 995.0	73.3	16 970.1	74.0
5	16 925.6	68.2	16 927.1		16 909.1	

[a]All peak positions are obtained by single voigt (n = 0), double voigt (n = 1), or double gaussian (n = 2,3,4,5) fits. The column labeled E refers to the position of maximum intensity of the combined fit, while $E(Q_1)$ and $E(Q_2)$ refer to the maxima of the two components of which the fit consists. The ΔE columns show the difference between the peaks or peak components of n and n + 1. Because the fit for n = 5 is not considered to be reliable, ΔE is not given.

A fit was made to obtain more information about the positioning of the peaks. A background representing acoustic phonons was chosen by adding three wide gaussians (green line). On top of the background each peak was appointed one Voigt profile (for n = 0), two Voigt profiles (for n = 1), or two gaussians (for n = 2, 3, 4, 5, all red lines). The result of the total fit (orange line) is shown in Figure 1. An overview of the positions of the peaks and their fitted components is given in Table 1. While the fit with two profiles per peak is excellent, attempts to use more gaussians per peak resulted in too weak and wide gaussians with insignificant fit improvements.

This fit suggests that there are two progressions hidden in the emission spectrum, with different but similar energies. The excellent fit of the n = 1 peak with two lines corresponding to the emission to the (n_1,n_2) vibrational levels (1,0) and (0,1) makes this clear. The n = 2 peak then is expected to be made of three emission lines to the vibrational levels (2,0), (1,1), and (0,2). The position of the expected (1,1) line is indicated with a black arrow in Figure 1. Because this line is expected to lie between the (2,0) and (0,2) lines, inspection of the figure suggests the assignment of the two gaussians to the (2,0) and (0,2) emissions. The same argument as applied to the n = 3 peak and the (3,0), (2,1), (1,2), and (0,3) lines suggests the assignment of the two gaussians to the (3,0) and (0,3) emissions. The positions of the expected (2,1) and (1,2) lines are indicated. As the peaks in the experiment are all well represented by their two-profile fits and because there is no clear indication in the spectrum that any of the gaussians represents a combined vibration (n_1,n_2) (with n_1 and n_2 not equal to 0), the conclusion is drawn that these cross peaks do not have significant intensity to be observed and are therefore difficult to include in the fit. This gives rise to some uncertainty in the present fits.

In Table 1, the low energy progression (Q_1) shows an alternating energy difference between the energy of n and n + 1, which might correspond to some irregularity in its vibration potential. The high energy progression (Q_2) shows a steady decrease in energy difference between n and n + 1, which can be caused by an anharmonicity in the vibration potential. To gain further insight into the two experimentally observed vibrations, ab initio calculations were performed.

III. AB INITIO CALCULATIONS

A. Method. We performed ab initio wave function theory embedded cluster quantum chemical calculations on the $(BiO_9)^{16-}$ cluster embedded in the SrB_4O_7 host with the MOLCAS suite of programs.[10] In brief, these are SA-CASSCF/MS-CASPT2/RASSI-SO DKH calculations. The state-average complete-active-space self-consistent-field method (SA-CASSCF)[11−13] is used to handle nondynamic correlation due to near degeneracies; the multistate second-order perturbation theory method (MS-CASPT2)[14−17] is used next to handle dynamic correlation; and the restricted-active-space state-interaction spin−orbit method (RASSI-SO)[18,19] is used finally to take into account spin−orbit coupling effects. The second-order Douglas−Kroll−Hess Hamiltonian (DKH)[20,21] with the AMFI approximation of the DKH spin−orbit coupling operator[22] is used to consider relativistic effects. The embedding ab initio model potential (AIMP)[23] is used to consider Coulomb, exchange, and Pauli repulsion embedding effects from the SrB_4O_7 host onto the $(BiO_9)^{16-}$ cluster. All of the details are described in ref 8.

B. Potential Energy Surfaces. Bi^{2+} substitutes for Sr^{2+} in SrB_4O_7 [space group number 31, $Pmn2_1$ orthorhombic; a = 10.711 Å, b = 4.427 Å, c = 4.235 Å],[24] so that it occupies Sr 2(a) sites (y_{Sr} = 0.289, z_{Sr} = 0) of C_s point symmetry before lattice relaxation takes place. Its first coordination shell is made of 9 oxygens located as shown in Figure 2: one oxygen, O_a, is in the σ_{yz} symmetry plane, which is perpendicular to the a crystal axis; the remaining eight oxygens are four couples of symmetry related off-plane oxygens, O_b, O_c, O_d, and O_e. In the unrelaxed

dx.doi.org/10.1021/jp503453y | J. Phys. Chem. C 2014, 118, 17932−17939

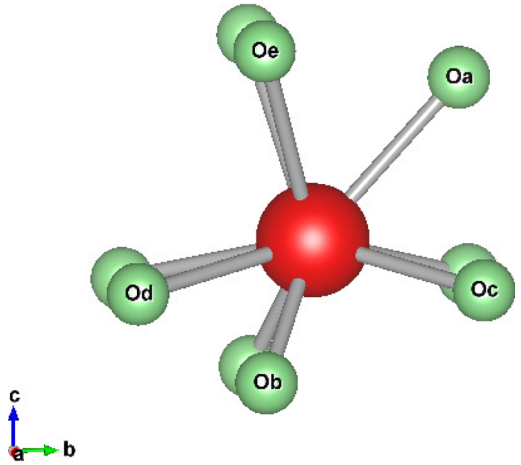

Figure 2. BiO_9 moiety. The *a*, *b*, and *c* axes of the SrB_4O_7 orthorhombic lattice are shown. O_a is in the symmetry plane, which is perpendicular to the *a* axis; O_b, O_c, O_d, and O_e are out of plane, and their symmetry related oxygens are unlabeled. The Bi−O distances in the unrelaxed host are Bi−O_a 2.73 Å, Bi−O_b 2.47 Å, Bi−O_c 2.68 Å, Bi−O_d 2.79 Å, and Bi−O_e 2.90 Å.

host, the Bi−O distances are Bi−O_a 2.73 Å, Bi−O_b 2.47 Å, Bi−O_c 2.68 Å, Bi−O_d 2.79 Å, and Bi−O_e 2.90 Å. As we can see in the figure, the projection of the oxygens on the *yz* symmetry plane is very asymmetric, and it does not seem to follow a regular pattern.

Taking into account the stiffness of the oxygen network of the tetraborate, the relatively large volume of the O_9 cage, and the low symmetry of the 2(a) site, we considered the hypothesis that Bi may experience an off-center displacement from the original site and that the $^2P_{1/2} \leftrightarrow {}^2P_{3/2}$ band profiles are mostly due to its vibration in the O_9 cage. According to this idea, we computed the potential energy surfaces along off-center displacements of Bi in the ground state, derived from $^2P_{1/2}$, and in the two first excited states, both of them derived from $^2P_{3/2}$.

Although spin−orbit coupling does not have important effects on equilibrium geometries and vibrational frequencies in many cases, like $4f^N$ and $4f^{N-1}5d$ configurations of lanthanide ions in solids,[25] it does here. The reason is that, as it was shown in ref 8, the three lowest states of the C_s $(BiO_9)^{16-}$ cluster embedded in the SrB_4O_7 host, $1E_{1/2}[^2P_{1/2}]$, $2E_{1/2}[^2P_{3/2}(1)]$, and $3E_{1/2}[^2P_{3/2}(2)]$, have strongly mixed characters of the ^2P related 1 $^2A''$, 1 $^2A'$, and 2 $^2A'$ spin−orbit free states, which have in turn very different angular natures because of their respective main configurational characters: 1 $^2A''$ is $a'(6s)^2a''(6p_x)$, 1 $^2A'$ is $a'(6s)^2a'(6p_y)$, and 2 $^2A'$ is $a'(6s)^2a'(6p_z)$. The shapes of these molecular orbitals are shown in Figure 3a. The *x* direction is perpendicular to the symmetry plane. The *y* and *z* directions are defined as perpendicular to the nodal planes of the $a'(6p_y)$ and $a'(6p_z)$

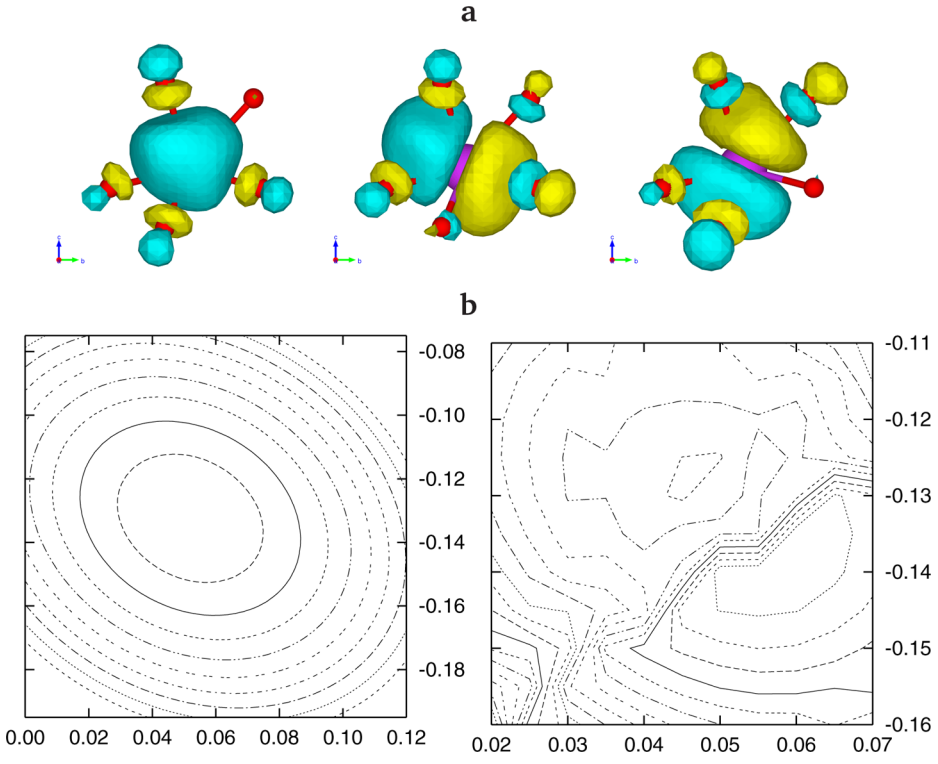

Figure 3. (a) $a''(6p_x)$, $a'(6p_y)$, and $a'(6p_z)$ natural orbitals as seen from the *a* crystal axis; the *b* (horizontal) and *c* (vertical) crystal axes are indicated with arrows; their orientation is the same as in Figure 2. The *x* and *a* axes are the same. The *y* and *z* axes are defined as perpedicular to the nodal planes of the orbitals $a'(6p_y)$ and $a'(6p_z)$, respectively. (b) $1\ E_{1/2}[^2P_{1/2}]$ ground-state energy surface corresponding to totally symmetric displacements of Bi (in Å) along the *b* direction (horizontal axes) and *c* direction (vertical axes). Left: Bidimensional cubic polynomial obtained by least-squares fitting of the total energies in a large area; energy isolines are shown every 20 cm^{-1} above the minimum. Right: Interpolation of the total energies in the region around the minimum, showing two nonequivalent minima and a 30 cm^{-1} energy barrier; 5 cm^{-1} isolines are shown. Note that the *b* and *c* crystal axes orientations in (a) and (b) coincide and that the scales in (b) are such that any oblique axis represented simultaneously in (a) and (b) will appear as two parallel lines.

dx.doi.org/10.1021/jp503453y | J. Phys. Chem. C 2014, 118, 17932−17939

natural molecular orbitals, respectively, and they are rotated around 30° clockwise with respect to the b and c crystal axes. Therefore, we cannot expect 1 ^{2}A″ and 1 $E_{1/2}$ to have the same equilibrium structure. Obviously, this also holds for 1 ^{2}A′ and 2 $E_{1/2}$ and for 2 ^{2}A′ and 3 $E_{1/2}$. In consequence with this, we performed the geometry optimizations at the spin−orbit coupling level of calculation.

Study of the Bi^{2+} perpendicular off-plane displacements along the x direction revealed that Bi^{2+} remains on plane. This result is the same when the spin−orbit coupling between the first 17 doublets and 3 quartets is allowed[8] and when only the spin−orbit coupling within the three $6s^26p-{}^2P$ related doublets is allowed. Within the vibrational degrees of freedom considered here, such displacement is a $Q_{a''}$ antisymmetric normal mode. Its computed ground-state harmonic vibrational frequency is $\omega_{a''}$ = 77 cm^{-1} (Table 2); the values in the two first excited states are 74 and 118 cm^{-1}, respectively.

Table 2. Experimental and Calculated Harmonic Vibrational Frequencies and Vibrational Barriers Corresponding to Symmetric a' and Antisymmetric a'' Off-Center Displacements of Bi^{2+}[a]

	on-plane a'			off-plane a''
state	$1a'$ barrier	$\omega_{1a'}$	$\omega_{2a'}$	$\omega_{a''}$
	Experiment			
$1E_{1/2}[^2P_{1/2}]$		∼73	89	
	Ab Initio Calculation			
$1E_{1/2}[^2P_{1/2}]$	30	93	121	77
$2E_{1/2}[^2P_{3/2}(1)]$	40	86	135	74
$3E_{1/2}[^2P_{3/2}(2)]$		102	131	118

[a]All numbers are in cm^{-1}.

Geometry optimization of the Bi^{2+} displacements along the b and c crystal axes in the ground state, using 0.05 Å steps and considering spin−orbit coupling between 17 doublets and 3 quartets, also gave the same results than when only the spin−orbit coupling between the three ^{2}P related states was considered. We then used a finer grid (0.005 Å) in the spin−orbit coupling calculation between 1 ^{2}A″, 1 ^{2}A′, and 2 ^{2}A′, to compute the potential energy surfaces around their minima. The results for the $1E_{1/2}[^2P_{1/2}]$ ground state are shown in Figure 3b. In the left-hand box we represent the bidimensional cubic polynomial obtained by least-squares fitting to the total energies evaluated at the grid points; 20 cm^{-1} equispaced isolines are shown. With this resolution, it is a slightly anharmonic envelope around the region of an apparent minimum at δ_{b0} = (0.05 ± 0.01) Å, δ_{c0} = (−0.13 ± 0.01) Å, where δ_{b0} and δ_{c0} are the Bi^{2+} off-center displacements from the original Sr^{2+} site along the b and c axes. The two symmetric normal modes that result from the analysis of the ground-state potential energy surface are clearly seen in the figure as the main axes of the quasi-elliptical energy isolines, and they are $Q_{1a'} = 0.87(\delta_b - \delta_{b0}) - 0.50(\delta_c - \delta_{c0})$ and $Q_{2a'} = 0.50(\delta_b - \delta_{b0}) + 0.87(\delta_c - \delta_{c0})$. Here, $(\delta_b - \delta_{b0})$ and $(\delta_c - \delta_{c0})$ are the displacements of Bi^{2+} from its equilibrium position along the b and c axes. These normal modes correspond to a 30° clockwise rotation of the δ_b and δ_c displacements (cos 30° = 0.87, sin 30° = 0.50). With this definition, the envelope of the ground-state potential energy surface can be written, up to second order, as the sum of squares $E = E_e + 1/2(k_{1a'}Q_{1a'}^2) + 1/2(k_{2a'}Q_{2a'}^2)$. It is remarkable that the symmetric normal mode Bi displacements are along directions very similar to the y and z directions of the molecular natural orbitals $a'(6p_y)$ and $a'(6p_z)$ (cf., Figure 3). We may then label the normal vibrations as $Q_y \equiv Q_{1a'}$ and $Q_z \equiv Q_{2a'}$. The two corresponding normal mode harmonic vibrational frequencies are $\omega_y \equiv \omega_{1a'}$ = 93 cm^{-1} and $\omega_z \equiv \omega_{2a'}$ = 121 cm^{-1} (cf., Table 2).

In the right-hand box of Figure 3b, we see further details of the minimum region, with 5 cm^{-1} equispaced isolines. Interestingly, instead of a harmonic minimum, there are two minima with different depths separated by a 30 cm^{-1} high energy barrier for the Bi^{2+} displacement along a direction very close to the y direction. The cubic fitting of a larger area could not detect its existence because of the small height of the barrier. The barrier has an undulating shape. The lowest minimum is located at off-center displacements δ_b = 0.058 Å, δ_c = −0.136 Å; the other minimum is 20 cm^{-1} higher in energy and located at δ_b = 0.045 Å, δ_c = −0.129 Å.

The results of an equivalent study of the potential energy surfaces of the first and second excited states, $2E_{1/2}[^2P_{3/2}(1)]$ and $3E_{1/2}[^2P_{3/2}(2)]$, are shown in Figure 4 and Table 2 together with those of the ground state. As the ground state, the first excited state has a lower minimum at δ_b = 0.030 Å, δ_c = −0.160 Å, and a higher minimum 35 cm^{-1} above and separated by a 40 cm^{-1} barrier, located at δ_b = 0.017 Å, δ_c = −0.152 Å. The second excited state does not show any energy barrier.

Let us comment on what can produce the energy barriers. The movement of Bi within the O_9 cage takes place with an increment of some Bi−O distances and a decrement of others. This happens in an ordered way for the off-plane a'' antisymmetric displacements along the x direction, because the existence of a symmetry plane at equilibrium forces the coordinated decrease of four Bi−O distances and increase of four Bi−O related distances, while the Bi−O_a distance increases. However, for the Bi^{2+} in-plane a' symmetric displacements, the balance of increments and decrements is complex because of the lack of symmetry in the distribution of oxygens along the b and c directions. We then may expect the corresponding balance of Bi−O ionic interactions to be complex as well and to be ultimately responsible for the appearance of the energy barrier along the y direction and for the fact that this barrier has a wavy shape.

It is also interesting to observe in Table 3 that the off-center displacements in the ground state bring Bi significantly closer to the closest four oxygens to the original Sr site, O_b and O_c (almost 0.1 Å), and more distant from all other oxygens, enhancing the formation of a BiO_4 pyramid. This is also true in the first excited state (except that the Bi−O_d distance also experiences a small reduction) and in the second excited state, where the formation of a BiO_4 pyramid is further enhanced.

C. Ab Initio Emission Spectrum Scenario. The picture that the ab initio calculations provide for the ground-state potential energy surface is one in which Bi^{2+} is shifted with respect to its on-center substitutional site toward the formation of a BiO_4 pyramid, and its vibration around its off-center minimum can be described as made of three slightly anharmonic modes with vibrational frequencies near 100 cm^{-1} and the following distribution: One of them is antisymmetric a'' and has the lowest frequency, the other two are symmetric a', and the less energetic of them has a double minimum with an energy barrier of about one-third of the vibrational frequency. Therefore, because the dominant contribution to the vibrational structure of the emission spectra comes from the totally symmetric modes, we must expect it to

dx.doi.org/10.1021/jp503453y | J. Phys. Chem. C 2014, 118, 17932−17939

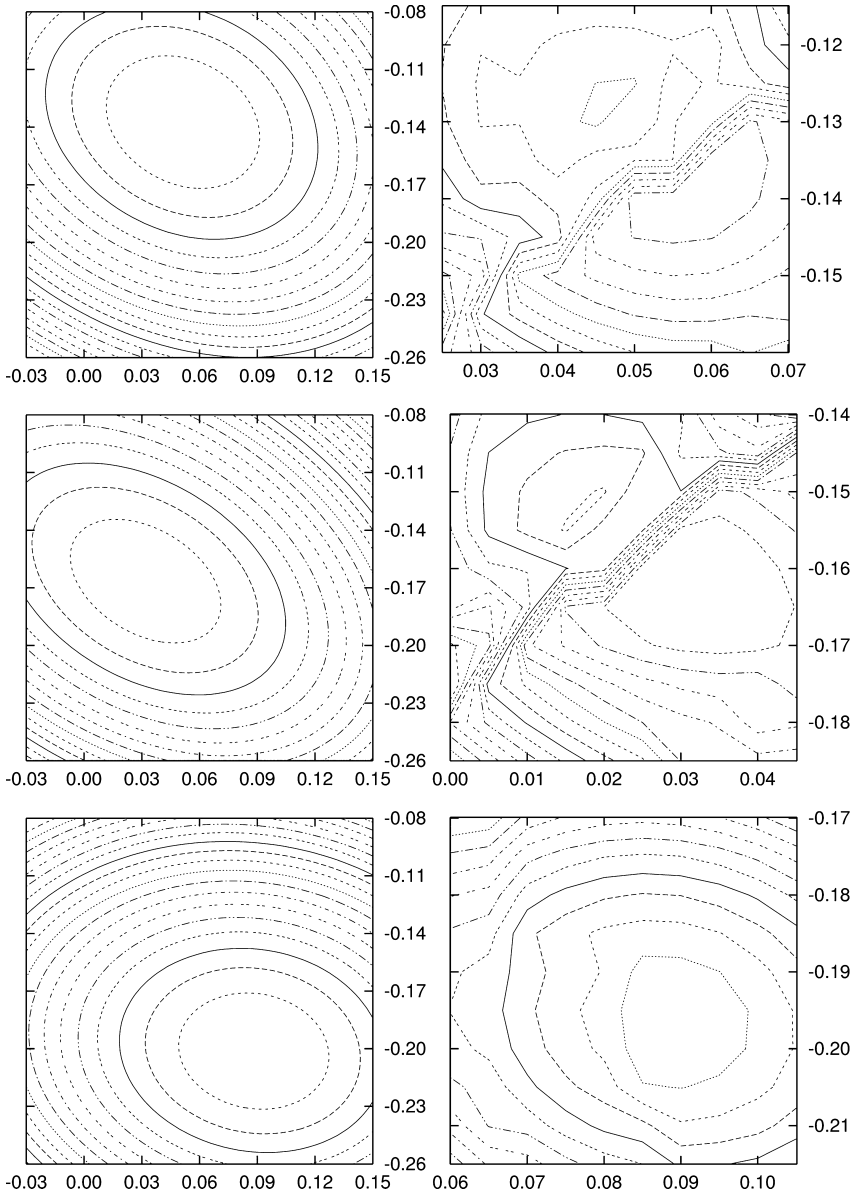

Figure 4. Potential energy surfaces of the three lowest states, $1E_{1/2}[^2P_{1/2}]$ (top), $2E_{1/2}[^2P_{3/2}(1)]$ (middle), and $3E_{1/2}[^2P_{3/2}(2)]$ (bottom), corresponding to on-plane displacements of Bi along the *b* direction (horizontal axes) and *c* direction (vertical axes), in Å. Left: Cubic fittings of the computed quasi-paraboloid enveloppes; 20 cm^{-1} equispaced isolines are shown. Right: Course grain interpolation of the computed energies in the regions around the envelope minima; 5 cm^{-1} equispaced isolines are shown.

be made of two vibrational progressions with intervals of around 100 cm^{-1}, the most energetic of them being a regular, slightly decreasing sequence, and the less energetic of them having some irregularities or anomalies associated with the small energy barrier.

The potential energy surfaces of the first and second excited states, which are responsible for absorption and excitation spectra band profiles, have the same basic features as the ground state, with the following differences: The first excited state has a larger $\omega_{2a'}$ and a slightly larger barrier (about one-half of its vibrational frequency); the three vibrational frequencies of the second excited state are larger, and it does not have an energy barrier. The high-resolution vibrational profile of the first absorption band then should be expected to be as complex as the emission profile, whereas the one of the second absorption must be simpler. The equilibrium offset with respect to the ground state is larger in the second excited state than in the first; this would be consistent with a wider second absorption band with a less pronounced fine structure, in agreement with experiment.[8]

IV. DISCUSSION OF THE HIGH-RESOLUTION EMISSION SPECTRUM

The analysis of the high-resolution emission profile in terms of two progressions (section II.B) agrees well with the scenario of two totally symmetric active modes for the emission spectrum found in the ab initio calculations (section III.C).

According to this, we modeled the experimentally found vibrational energy levels of the ground state (Table 1) by means of a first harmonic oscillator with a Gaussian energy barrier as high as one-third of its vibrational frequency, which was located in several positions, to model the lowest energy mode Q_1; and a second harmonic oscillator with a quartic anharmonic correction to model the highest energy mode Q_2

dx.doi.org/10.1021/jp503453y | J. Phys. Chem. C 2014, 118, 17932−17939

Table 3. Off-Center Displacements of Bi^{2+} along the *b* and *c* Crystal Axes with Respect to the Sr Site of SrB_4O_7, δ_b and δ_c, and Bi−O Distances Corresponding to the Deepest Potential Energy Surface Minimum of the Three Lowest States As Resulting from the Ab Initio Calculations[a]

		off-center sites		
	on-center site[b]	$1E_{1/2}$	$2E_{1/2}$	$3E_{1/2}$
	Off-Center Displacements			
δ_b	0.000	0.058	0.030	0.090
δ_c	0.000	−0.136	−0.160	−0.195
	Bi−O Distances			
$d(Bi-O_a)$	2.73	2.79	2.83	2.91
$d(Bi-O_b)$	2.47	2.39	2.36	2.36
$d(Bi-O_c)$	2.68	2.60	2.62	2.56
$d(Bi-O_d)$	2.79	2.81	2.78	2.82
$d(Bi-O_e)$	2.90	3.02	3.04	3.08

[a]All numbers are in angstroms. [b]Experimental data from ref 24.

(cf., Figure 5). In these calculations, we used perturbation theory up to the fourth order, and we found convergence in the level energies in all cases.

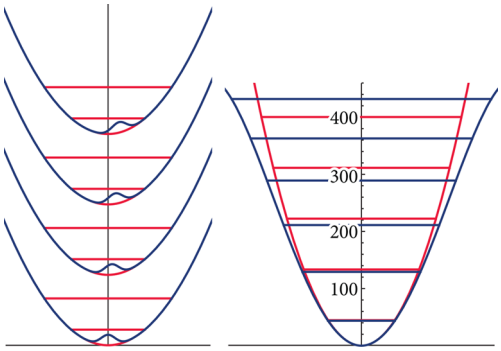

Figure 5. Left: Harmonic oscillator potential perturbed with low energy barriers in different locations, which illustrate the Q_1 mode. The corresponding vibrational energy levels of the harmonic oscillator are shown (gray inline). Right: Anharmonic potential used to match the vibronic coupling Q_2. The underlying harmonic oscillator potential is also shown (gray inline); it has a harmonic vibration frequency of 89 cm^{-1}.

Figure 6 shows the resulting energy separations for these perturbed harmonic potentials, as compared to the experimentally found separations. The mode with the quartic anharmonic perturbation agrees well with the experimentally found mode Q_2, and this mode is therefore assigned as $Q_{2a'}$.

The potential with the barrier causes an alternating energy increment, which is very characteristic and is also seen in the experimentally observed mode Q_1. The position of the barrier has an influence on the precise values of the energy increments. This variability means that the experimental data cannot provide full details of harmonic vibrational frequency, anharmonicity, barrier height, and barrier locations. Nevertheless, it provides the following structural information: the harmonic vibrational frequency is very close to 73 cm^{-1}, the anharmonicity is small up to 400−500 cm^{-1}, and there is an energy barrier of around one-third of the vibrational frequency whose location is not necessarily in the center of the oscillator. This mode is assigned as $Q_{1a'}$.

Finally, it is interesting to estimate the Huang−Rhys vibronic coupling parameter *S* and compare it with ab initio calculated

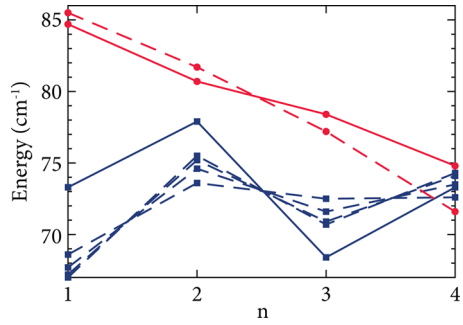

Figure 6. Energy increments in the $(0,n_2)$ sequence (red lines) and $(n_1,0)$ sequence (blue lines) from experiment (solid lines) and from the calculated perturbed potentials (dashed lines). The red dashed line shows the results for a harmonic potential of vibrational frequency 89 cm^{-1} with a small quartic perturbation, which we compare with Q_2 (the red solid line). The blue dashed lines show the results for a harmonic potential of vibrational frequency 73 cm^{-1} with a barrier of one-third of the vibrational frequency, with positions corresponding to Figure 5. The strongest alternating behavior corresponds to a symmetric barrier. We compared this mode with Q_1 (the blue solid line).

values. An effective-mode analysis of the intensity ratio between the two first peaks using $I(n) =\propto e^{-S}S^n/n!$ gives the Huang−Rhys parameter $S = 1.32$.[26] According to its definition, this parameter can give the absolute value of the effective mode offset between the exicted state and the ground state, ΔQ:

$$S = \frac{1}{2}\frac{M\omega^2}{\hbar\omega}(\Delta Q)^2 \quad (1)$$

Here, *M* is the reduced mass of the oscillator, which is the mass of bismuth in this case. The result is $|\Delta Q| = 0.075$ Å, which can be identified with the displacement experienced by Bi after the $2E_{1/2}[^2P_{3/2}(1)] \rightarrow 1E_{1/2}[^2P_{1/2}]$ emission. The ab initio displacement is 0.037 Å, which is an underestimation of the experimental value. This underestimation is qualitatively in line with previous ab initio results for f−d transitions in f-elements, where also the experimentally determined displacement was higher than the value obtained from ab initio calculations.[25,27]

The result that the experiment and calculations agree on the order of magnitude of the displacement is a confirmation that the vibrational modes observed in the spectrum correspond to vibration of Bi in a rigid O_9 cage. A local vibrational mode that involves displacements of the coordinating oxygen ions would have a reduced mass *M* that is at least 1 order of magnitude smaller.

An equivalent analysis can be made on the progressions of the individual modes, although the results are expected to be less precise due to the uncertainties of the individual fitted intensities. Such an analysis gives individual mode Huang−Rhys parameteres $S_1 = 0.94$ and $S_2 = 0.35$, and individual mode offsets between ground and excited state $|\Delta Q_1| = 0.064$ Å and $|\Delta Q_2| = 0.036$ Å. These results mean a larger displacement of Bi after the emission along the mode with a lower frequency and an energy barrier (mode Q_1) than along the mode with a higher frequency and no barrier (mode Q_2).

The ab initio results are $\Delta Q_1 = -0.012$ Å and $\Delta Q_2 = -0.035$ Å. Although there is a good agreement for Q_2, there is a significant discrepancy for Q_1. There is however a better agreement ($\Delta Q_1 = -0.027$ Å) when the displacement is calculated for the second, slightly higher energy, minimum of the excited state $2E_{1/2}[^2P_{3/2}(1)]$, which indicates that the true

dx.doi.org/10.1021/jp503453y | J. Phys. Chem. C 2014, 118, 17932−17939

minimum of the excited state is the one that the ab initio calculation gives as slightly higher in energy. This would not be surprising bearing in mind the very small energy differences between the minima at both sides of the barrier along Q_1 in both states. Such a switch of the true minimum would also be consistent with the underestimation of the effective mode offset.

V. CONCLUSIONS

The fine structure of the 4.2 K emission band corresponding to the $6s^26p$ intraconfigurational $2E_{1/2}[^2P_{3/2}(1)] \rightarrow 1E_{1/2}[^2P_{1/2}]$ transition of Bi^{2+} in the Sr C_s site of SrB_4O_7 (refs 1, 8) has been measured with high resolution. Its vibrational structure consists of two line progressions, one with regularly decreasing intervals starting in 85 cm^{-1} and another with alternating intervals starting in 73 cm^{-1}. On the basis of potential energy surfaces of ab initio calculations, the fine structure has been interpreted as due to two totally symmetric a' off-center vibrations of Bi^{2+}. Their normal mode harmonic vibrational frequencies were found to be 73 and 89 cm^{-1}. The lowest vibrational normal mode is hindered by a low energy barrier of about one-third of its vibrational frequency, which is responsible for the irregularities of the line intervals.

SA-CASSCF/MS-CASPT2/RASSI-SO ab initio calculations of the potential energy surfaces that correspond to Bi^{2+} off-center displacements in the three lowest states of a C_s symmetry $(BiO_9)^{16-}$ cluster embedded in the SrB_4O_7 host have been performed. Bi^{2+} is found to stay in-plane in the $6s^26p$ $1E_{1/2}[^2P_{1/2}]$ ground state, with a a'' off-plane vibrational frequency of $\omega_{a''} = 77$ cm^{-1}, and to have two a' in-plane normal modes with frequencies $\omega_{1a'} = 93$ cm^{-1} and $\omega_{2a'} = 121$ cm^{-1}. The latter frequencies are to be compared to the 73 and 89 cm^{-1} obtained from the experimental emission spectrum. The quantitative deviations are reasonable, and they can be attributed to the assumption of a rigid lattice in which Bi^{2+} vibrates and to the practical limitations of the performed ab initio calculations. The respective normal modes are found to be Bi^{2+} displacements along directions almost parallel to the main axes of the $a'(6p_y)$ and $a'(6p_z)$ natural orbitals. The two first excited states $2E_{1/2}[^2P_{3/2}(1)]$ and $3E_{1/2}[^2P_{3/2}(2)]$ also have their energy minima on-plane and off-center. They both have vibrational frequencies similar to the ground state. The first excited state also has two minima separated by a low energy barrier. This is not the case in the second excited state.

The details of the off-center vibrations of Bi^{2+} in SrB_4O_7 have been unveiled as a result of the complementarity between high-resolution spectroscopy and ab initio calculations.

AUTHOR INFORMATION

Corresponding Author

*Phone: +34670099687. E-mail: luis.seijo@uam.es.

Notes

The authors declare no competing financial interest.

ACKNOWLEDGMENTS

This work was partly supported by a grant from Ministerio de Economa y Competitivad, Spain (Dirección General de Investigación y Gestión del Plan Nacional de I+D+I, MAT2011-24586), and by the EU Marie Curie Initial Training Network LUMINET (316906).

REFERENCES

(1) Blasse, G.; Meijerink, A.; Nomes, M.; Zuidema, J. Unusual Bistmuth Luminescence in Strontium Tetraborate (SrB_4O_7:Bi). *J. Phys. Chem. Solids* **1994**, *55*, 171−174.

(2) Srivastava, A. M. Luminiscence of Divalent Bismuth in $M^{2+}BPO_5$ (M^{2+}=Ba^{2+}, Sr^{2+} and Ca^{2+}). *J. Lumin.* **1998**, *78*, 239−243.

(3) Peng, M.; Wondraczek, L. Bi^{2+}-Doped Strontium Borates for White-Light-Emitting Diodes. *Opt. Lett.* **2009**, *34*, 2885−2887.

(4) Peng, M.; Wondraczek, L. Photoluminescence of $Sr_2P_2O_7$:Bi^{2+} as a Red Phosphor for Additive Light Generation. *Opt. Lett.* **2010**, *35*, 2544−2546.

(5) Bai, Z.; Fujii, M.; Hasegawa, T.; Kitano, S.; Imakita, K.; Mizuhata, M.; Hayashi, S. Co-existence of Bi with Multiple Valence States in Zeolites. Controlling the Optical Properties by Annealing Atmosphere. *Opt. Mater.* **2012**, *34*, 821−825.

(6) Peng, M.; Lei, J.; Li, L.; Wondraczek, L.; Zhang, Q.; Qiu, J. Site-Specific Reduction of Bi^{4+} to Bi^{2+} in Bismuth-Doped Over-Stoichioemetric Barium Phosphates. *J. Mater. Chem. C* **2013**, *1*, 5303−5308.

(7) Cao, R.; Zhang, F.; Liao, C.; Qiu, J. Yellow-to-Orange Emission from Bi^{2+}-Doped RF_2(R=Ca and Sr) Phosphors. *Opt. Express* **2013**, *21*, 15728−15733.

(8) de Jong, M.; Meijerink, A.; Gordon, R. A.; Barandiarán, Z.; Seijo, L. Is Bi^{2+} Responsible for the Red-Orange Emission of Bismuth-Doped SrB_4O_7? *J. Phys. Chem. C* **2014**, *118*, 9696−9705.

(9) Blasse, G.; Meijerink, A.; Nomes, M.; Zuidema, J. Unusual Bismuth Luminescence in Strontium Tetraborate (SrB_4O_7:Bi). *J. Phys. Chem. Solids* **1994**, *55*, 171−174.

(10) Karlström, G.; Lindh, R.; Malmqvist, P. A.; Roos, B. O.; Ryde, U.; Veryazov, V.; Widmark, P. O.; Cossi, M.; Schimmelpfennig, B.; Neogrady, P.; et al. MOLCAS: A Program Package for Computational Chemistry. *Comput. Mater. Sci.* **2003**, *28*, 222−239.

(11) Roos, B. O.; Taylor, P. R.; Siegbahn, P. E. M. A Complete Active Space SCF Method (CASSCF) Using a Density-Matrix Formulated Super-CI Approach. *Chem. Phys.* **1980**, *48*, 157−173.

(12) Siegbahn, P. E. M.; Heiberg, A.; Roos, B. O.; Levy, B. Comparison of the Super-CI and the Newton-Raphson Scheme in the Complete Active Space SCF Method. *Phys. Scr.* **1980**, *21*, 323−327.

(13) Siegbahn, P. E. M.; Heiberg, A.; Almlöf, J.; Roos, B. O. The Complete Active Space SCF (CASSCF) Method in a Newton-Raphson Formulation with Application to the HNO Molecule. *J. Chem. Phys.* **1981**, *74*, 2384−2396.

(14) Andersson, K.; Malmqvist, P.-A.; Roos, B. O.; Sadlej, A. J.; Wolinski, K. Second-Order Perturbation Theory with a CASSCF Reference Function. *J. Phys. Chem.* **1990**, *94*, 5483−5488.

(15) Andersson, K.; Malmqvist, P.-A.; Roos, B. O. Second-Order Perturbation Theory with a Complete Active Space Self-Consistent Field Reference Function. *J. Chem. Phys.* **1992**, *96*, 1218−1226.

(16) Zaitsevskii, A.; Malrieu, J.-P. Multi-Partitioning Quasidegenerate Perturbation Theory. A New Approach to Multireference Møller-Plesset Perturbation Theory. *Chem. Phys. Lett.* **1995**, *233*, 597−604.

(17) Finley, J.; Malmqvist, P.-A.; Roos, B. O.; Serrano-Andrés, L. The Multi-State CASPT2Method. *Chem. Phys. Lett.* **1998**, *288*, 299−306.

(18) Malmqvist, P. A.; Roos, B. O.; Schimmelpfennig, B. The RASSI Approach with Spin-Orbit Coupling. *Chem. Phys. Lett.* **2002**, *357*, 230−240.

(19) Paulovic, J.; Nakajima, T.; Hirao, K.; Lindh, R.; Malmqvist, P.-A. Relativistic and Correlated Calculations on the Ground and Excited States of ThO. *J. Chem. Phys.* **2003**, *119*, 798−805.

(20) Douglas, M.; Kroll, N. M. Quantum Electrodynamical Corrections to the Fine Structure of Helium. *Ann. Phys. (N.Y.)* **1974**, *82*, 89−155.

(21) Hess, B. A. Relativistic Electronic-Structure Calculations Employing a Two-Component No-Pair Formalism with External-Field Projection Operators. *Phys. Rev. A* **1986**, *33*, 3742−3748.

(22) Hess, B. A.; Marian, C. M.; Wahlgren, U.; Gropen, O. A Mean-Field Spin-Orbit Method Applicable to Correlated Wavefunctions. *Chem. Phys. Lett.* **1996**, *251*, 365−371.

(23) Barandiarán, Z.; Seijo, L. The Ab Initio Model Potential Representation of the Crystalline Environment. Theoretical Study of the Local Distortion on NaCl:Cu^{+}. *J. Chem. Phys.* **1988**, *89*, 5739−5746.
(24) Krogh-Moe, J. The Crystal Structure of Strontium Diborate $SrO.2B_2O_3$. *Acta Chem. Scand.* **1964**, *18*, 2055−2060.
(25) Gracia, J.; Seijo, L.; Barandiarán, Z.; Curulla, D.; Niemansverdriet, H.; van Gennip, W. Ab Initio Calculations on the Local Structure and the 4f-5d Absorption and Emission Spectra of Ce^{3+}-Doped YAG. *J. Lumin.* **2008**, *128*, 1248.
(26) Henderson, B.; Imbusch, G. F. *Optical Spectroscopy of Inorganic Solids*; Clarendon Press: Oxford, 1989.
(27) Sánchez-Sanz, G.; Seijo, L.; Barandiarán, Z. Electronic Spectra of Yb^{2+}-Doped $SrCl_2$. *J. Chem. Phys.* **2010**, *133*, 114506.